

Graphene Barristor, a Triode Device with a Gate-Controlled Schottky Barrier

Heejun Yang,^{1*} Jinseong Heo,^{1*} Seongjun Park,¹ Hyun Jae Song,¹ David H. Seo,¹ Kyung-Eun Byun,¹ Philip Kim,² InKyeong Yoo,¹ Hyun-Jong Chung,^{1†} Kinam Kim³

¹Graphene Research Center, Samsung Advanced Institute of Technology, Yongin 446-712, Korea.

²Department of Physics, Columbia University, New York 10027, USA. ³Samsung Advanced Institute of Technology, Yongin 446-712, Korea.

*These authors contributed equally to this work.

†To whom correspondence should be addressed. E-mail: hyunjong.chung@samsung.com

Despite several years of research into graphene electronics, sufficient I_{on}/I_{off} in graphene transistors with conventional device structures has been impossible to obtain. We report on a three-terminal active device, a graphene variable-barrier “barristor” (GB), where the key is an atomically sharp interface between graphene and hydrogenated silicon. Large modulation on the device current (on/off ratio of 10^5) is achieved by adjusting the gate voltage to control the graphene-silicon Schottky barrier. The absence of Fermi-level pinning at the interface allows the barrier’s height to be tuned to 0.2 electron volts by adjusting graphene’s work function, which results in large shifts of diode threshold voltages. Fabricating GBs on respective 150-mm wafers and combining complementary p- and n-type GBs, we demonstrate inverter and half-adder logic circuits.

The triode, composed of a diode and a grid in a vacuum tube, was the first three-terminal active device that had been used to amplify and to switch electric signals, which led the technical innovations for modern electronics in the early 20th century (1). Solid-state transistors and integrated circuits (ICs) based on silicon were more practical for complicated logic circuits and thus replaced triodes. Although silicon transistors have continued to improve their speed and integration density, they now near the potential limit where further reduction of channel length causes inevitable leakage currents (2). In order to present an alternative route for overcoming these challenges, we introduce a class of three-terminal device based on a graphene-silicon hybrid device that mimics a triode operation. The key device function takes place at the electrostatically gated graphene/silicon interface where a tunable Schottky barrier controls charge transport across a vertically stacked structure. We named this barrier variable device, which is a solid-state descendant of the triode, “barristor.”

Graphene is a zero-gap semiconductor whose Fermi energy can be adjusted by electrostatic gating owing to its two-dimensional (2D) nature (3–5). Because graphene is metallic at a sufficiently large Fermi energy, a Schottky barrier (SB) forms at the interface between the doped graphene and the semiconductor (6–10). However, SB between graphene and a well-controlled semiconductor surface, such as hydrogen-terminated Si, is different from a conventional metal-semiconductor SB in two important ways. First, the formation of interface states is suppressed in graphene-semiconductor junctions (11) because the interaction between chemically inert graphene and a completely saturated semiconductor surface i.e., without dangling bonds is negligible (12). Second, graphene’s work function (WF) can be adjusted electrostatically over a wide range by tuning the Fermi energy (E_F) via the electrostatic field effect (13, 14). We could realize a graphene barristor (GB) by combining these two effects.

A schematic diagram of the GB structure and its top view are shown in Fig. 1, A and B. Single-layer graphene in contact with the source electrode forms the SB at its interface with the silicon surface at the drain contact. Two kinds of GBs can be formed depending on the silicon doping type: n-type GB at n-type silicon and p-type GB at p-type silicon. We used transmission electron microscopy (TEM) to develop an optimal transfer process for graphene onto Si substrates in order to create atomically sharp interfaces (inset of Fig. 1C) which minimizes atomic defects or silicon dioxide formation that can create charge trapping sites. Figure 1C displays a typical Schottky diode characteristic of a p-type GB with an optimized graphene/Si interface. The forward characteristic at a low bias showed a diode ideality factor $\eta_{id} \approx 1.1$ for this particular device. The ideality factor we obtained in our GB is considerably better than those reported in exfoliated graphene-Si junctions (9), confirming the high interfacial quality in our GBs.

The recent availability of large-scale graphene growth through chemical vapor deposition (CVD) techniques (15–19) allowed us to integrate graphene devices at wafer scales using conventional semiconductor micro-fabrication processes (20). Large-scale integration has not been possible for similar devices such as p-n diodes demonstrated in highly customized and suspended semiconducting nanotubes (21, 22). We demonstrated integration of gate-tunable GB arrays on a 6 inch wafer by transferring a single-layer graphene grown by CVD (19, 23) onto a pre-patterned Si substrate. Figure 1D shows an array of 2,000 devices on a 6-inch (150-mm) wafer. At room temperature, the range of the ideality factor and the current density of GBs are found to be 1.1–4.0 and $10^1 \sim 10^4$ A/cm² respectively (see figs. S3 to S5 in the supplementary materials) (24), where the variation is due to the different wafer batches. These GB devices exhibited greater than 90% device yield with excellent uniformity in terms of device characteristics across the wafer with appropriate current level (fig. S2).

We could electrostatically modulate the graphene’s WF through the top gate electrode and gate dielectric above the graphene (14), which resulted in a variation on the SB height. Because the injection of the majority carriers from graphene to silicon is determined by the SB height ϕ_b , the top gate then directly controls the magnitude of the current across the source and the drain. The main panel of Fig. 2 shows the characteristic of p-type GB at various gate voltages (V_{gate}). The rectification behavior of the GB was demonstrated in that the GB current (I_{SD}) increased steeply as the bias voltage (V_{bias}) surpassed the “turn-on” voltage, V_{TO} . V_{TO} could be adjusted between 0 V and 1.3 V as V_{gate} was modulated between -5 V and 5 V, the range needed to keep this GB in p-type operation. Similar triode behavior was observed in n-type GBs (Fig. 2 inset), where the bias polarity was reversed because electrons become the majority carrier. The large modulation of the GB current was indicative of a large variation in the SB height, caused by the electric field effect (EFE) from V_{gate} .

In order to quantitatively analyze the device characteristic, we used

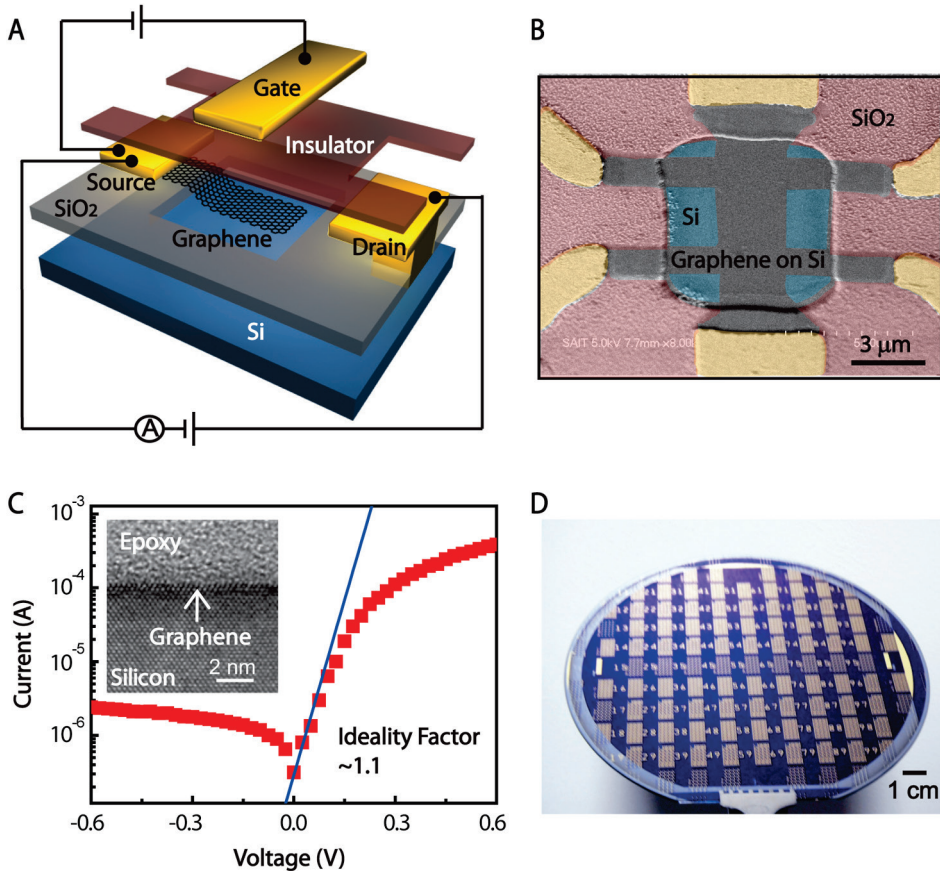


Fig. 1. Graphene Barristor. **(A)** A schematic diagram to show the concept of a GB. **(B)** False colored scanning electron microscopy image of the GB before the top gate fabrication process. **(C)** Current versus bias voltage characteristic of a GB at a fixed gate voltage $V_{\text{gate}} = 0$ V, showing a Schottky diode characteristic. The inset shows a transmission electron microscope image of graphene/silicon junction. No native oxide or defect is seen in the image. **(D)** A photograph of ~2000 GB arrays implemented on a 6 inch wafer.

the diode equation

$$I = AA^*T^2 \exp\left(\frac{-q\phi_b}{k_B T}\right) \left[\exp\left(\frac{qV_{\text{bias}}}{\eta_{\text{id}} k_B T}\right) - 1 \right]$$

where A is the area of the Schottky junction, A^* is the effective Richardson constant, q is the elementary charge, k_B is the Boltzmann constant, and T is the temperature. Quantitative analysis of the SB height ϕ_b can be done by investigating the temperature dependence of the GB current in the reverse bias saturation regime [$\exp(qV_{\text{bias}}/\eta_{\text{id}} k_B T) \ll 1$]. Here, the diode current becomes insensitive to V_{bias} and $I_{\text{sat}} \propto T^2 \exp(-q\phi_b/k_B T)$. Figure 3A shows a plot of $\ln(I_{\text{sat}}/T^2)$ vs. $q/k_B T$ in the reverse bias saturation regime. We estimated the SB height ϕ_b for a given gate voltage V_{gate} from the slope of each curve. Figure 3B shows the resulting SB heights obtained as a function of V_{gate} . V_{gate} in-

creased from 0 to 5 V, while ϕ_b decreased substantially from 0.45 eV to 0.25 eV. We attributed the drastic change in ϕ_b to the EFE induced Fermi level change, ΔE_F . Indeed, as shown in Fig. 3B the measured variation of ϕ_b , $\Delta\phi_b = \phi_b - \phi_b(\Delta E_F = 0)$, was well correlated to the change of ΔE_F , obtained independently by converting the measured Hall carrier density (n_H) using $\Delta E_F = \hbar v_F \sqrt{\pi n_H}$, where $v_F = 10^6$ m/sec was used for the Fermi velocity of graphene. We observed that $\Delta\phi_b \approx -\Delta E_F$ for a wide range of V_{gate} (fig. S7), which suggests that the WF modulation of graphene in the absence of Fermi-level pinning is fully responsible for the variation of ϕ_b as depicted in Fig. 3C and 3D.

The absence of Fermi-level pinning, one of the major sources for high device resistance in silicon electronics (25), comes from the suppression of the surface states at the interface of silicon and graphene. In our GB, we could eliminate the “Fermi-level pinning” and manipulate the SB height as in the ideal Schottky-Mott limit (Fig. 3B), where the SB height is controlled through the selection of metal and semiconductor with appropriate WFs (26, 27).

Two different types of GB operations are possible, as shown in Fig. 4A. The first type uses the GB in the reverse-biased regime (orange shaded region in Fig. 4A). Here, a conventional FET-like device operation could be possible; i.e., the GB current, I , had the tendency to saturate at large reverse bias voltages, and the “on” current, I_{on} , had been modulated by V_{gate} . The off state current, I_{off} , was determined at the greatest attainable SB, which yielded an $I_{\text{on}}/I_{\text{off}} \sim 300$ in Fig. 4A. The second type of operation could be realized by using the device in the forward biasing region (the blue shaded region in Fig. 4A). In this regime, the diode current did not saturate as V_{bias} increased, but deviated from a typical FET-like device operation. However, near the diode turn-on regime, I varied by several orders of magnitude as V_{gate} changed, resulting in a switching operation with a large $I_{\text{on}}/I_{\text{off}}$ ratio. Figure 4B shows the switching characteristic of the diode current in a forward biased p-type GB, demonstrating a remarkably high $I_{\text{on}}/I_{\text{off}} \sim 10^5$. We note that the large $I_{\text{on}}/I_{\text{off}}$ ratio and small off-current overcame the key obstacle in graphene-based electronics.

Three terminal operation of GB offers various integrated device functionalities. Similar to the CMOS inverter operation, a series connection of n- and p-type complementary GBs inverted the input signal V_{in} to its inverse V_{out} (Fig. 4C). The low V_{out} originated from the high on/off current ratio of GBs implying that only a small amount of static off-state power would be consumed. As for more complicated logic applications, we demonstrated a half-adder circuit built from n- and p-type 10 GBs. The schematic with two inputs (A and B) and two outputs (SUM and CARRY) is shown in Fig. 4D. The measured output voltage levels are represented in Fig. 4E. These results suggest that the GB can provide a route to realize high speed logic applications (28, 29) based on graphene-semiconductor hybrid devices.

In conclusion, our GB suggests the possibility of a graphene logic device by achieving a high on/off ratio of $\sim 10^5$, which exceeds the minimum requirement for logic transistors. Furthermore, the on/off ratio and the current density can be improved with well-developed semi-conductor processes since there is not a fundamental (or structural) limit. GB also has an advantage in lateral scaling as the barrier is formed vertically.

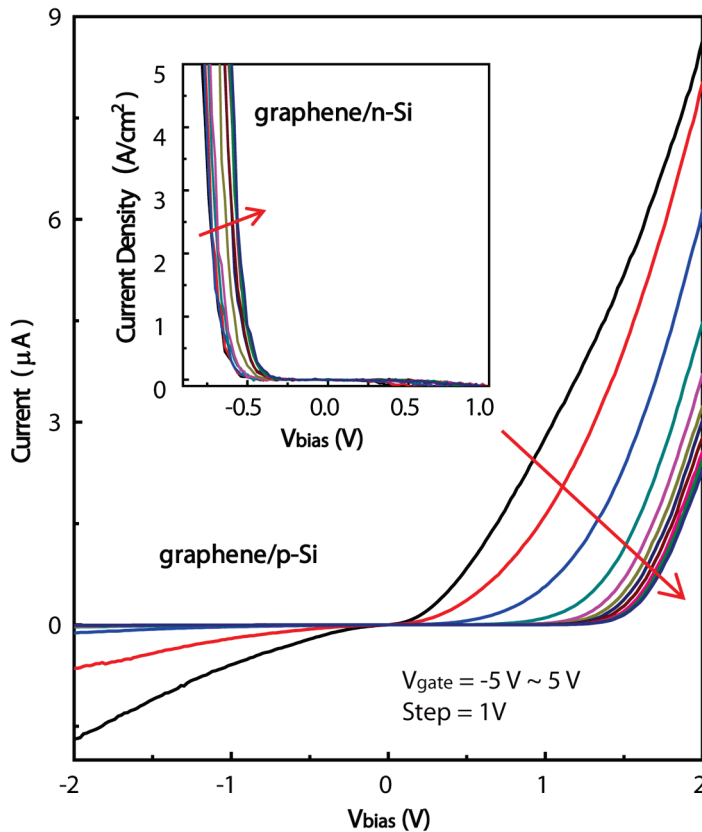
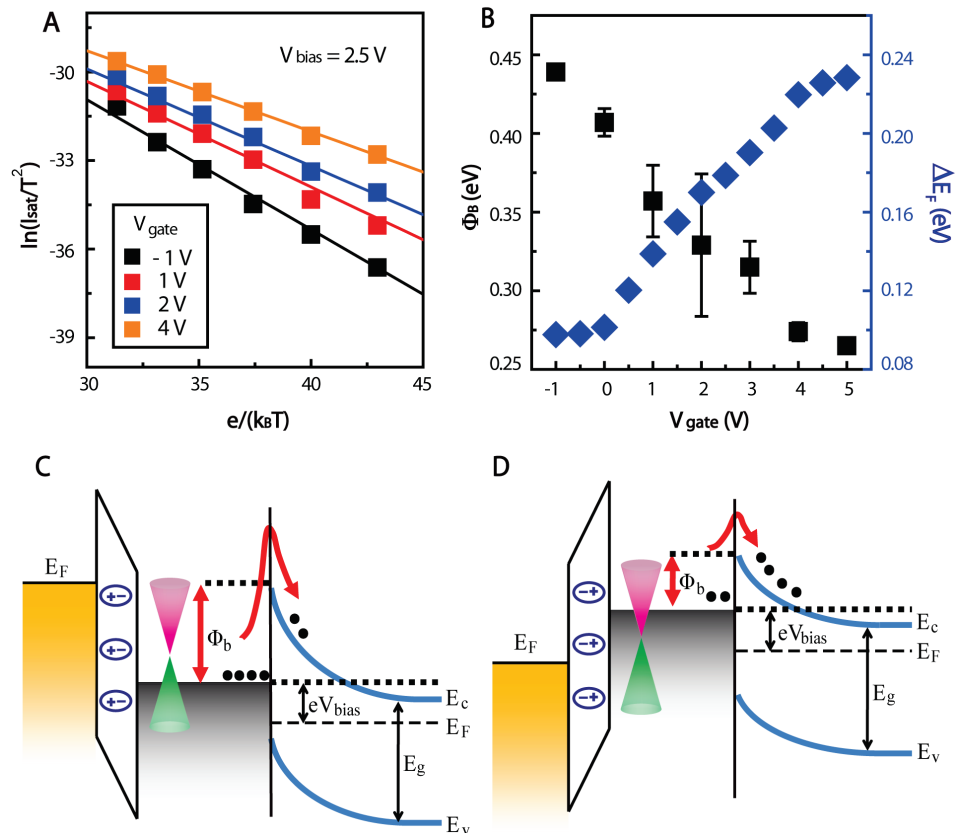


Fig. 2. Graphene barristor characteristics. The current and bias voltage characteristics of p-type (main panel) and n-type (inset) GBs at various fixed V_{gate} values. V_{gate} varies in the range -5 to 5 V with step size of 1 V for each curve. Red arrow indicates the direction of increasing V_{gate} .

Fig. 3. (A) Temperature dependent diode characteristic. The saturation current of the n-type GB, I_{sat} is obtained by measuring the current at $V_{\text{bias}} = 2.5$ V at various temperature and gate voltage values. Different colors used for different V_{gate} from -1 V to 4 V with 1~2 V step variation. The line fit for each V_{gate} value is drawn to yield the Schottky barrier height from the slope of the fitted line. **(B)** The SB height obtained from the fit in (A) as a function of V_{gate} (black squares, left axis). The graphene Fermi energy on the right axis is obtained from Hall measurement at the same gate voltage V_{gate} . Monotonic increase (decrease) of observed SB height from the fit in (A) as a function of V_{gate} (black squares, left axis). The graphene Fermi energy on the right axis is obtained from Hall measurement at the same gate voltage V_{gate} . Monotonic increase (decrease) of observed SB height consists with band diagram in Fig. 3C (3D). **(C and D)** Schematic band diagrams of GB with the electric field effect generated by the gate on the top of graphene. Applying negative voltage on the gate induces holes in graphene, increasing its work function and increasing the Schottky barrier height. As a result, the reverse current across the Schottky barrier decreases (C). Positive gate voltage decreases the Schottky barrier height and increases reversed current (D).



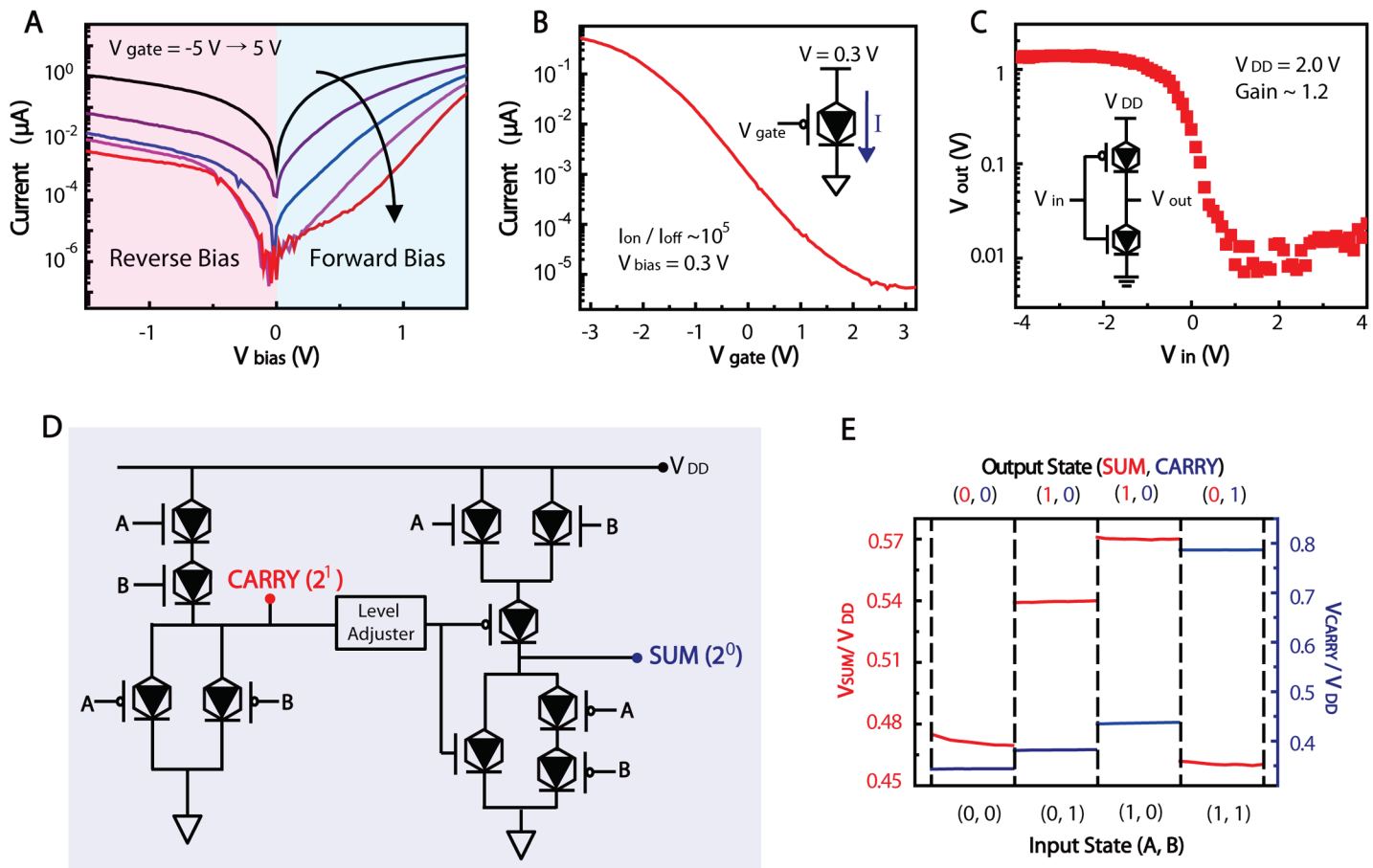


Fig. 4. (A) Switching behavior of p-type GB in reverse (orange background) and forward (blue background) bias regimes. The GB current is plotted against the source drain bias at various fixed gate voltages. V_{gate} varies in the range of $-5 \text{ V} \sim 5 \text{ V}$ with a step of $\sim 2 \text{ V}$. Black arrow indicates the direction of increasing V_{gate} . (B) The forward diode current as a function of gate V_{gate} at fixed bias $V_{\text{bias}} = 0.3 \text{ V}$. Unipolar control of forward current with the ratio of 10^5 is obtained. (C) Inverter characteristics obtained from integrated n- and p-type GBs and schematic circuit diagram for the inverter. V_{DD} is connected to p-type GB and the gain of the inverter is ~ 1.2 . (D) Schematic of circuit design of a half-adder implemented with n- and p-type GBs. (E) Output voltage levels for SUM and CARRY for four typical input states.

References and Notes

1. J. Bardeen, W. H. Brattain, The transistor, a semi-conductor triode. *Phys. Rev.* **74**, 230 (1948). [doi:10.1103/PhysRev.74.230](https://doi.org/10.1103/PhysRev.74.230)
2. M. Lundstrom, Moore's law forever? *Science* **299**, 210 (2003). [doi:10.1126/science.1079567](https://doi.org/10.1126/science.1079567) Medline
3. K. S. Novoselov *et al.*, Two-dimensional gas of massless Dirac fermions in graphene. *Nature* **438**, 197 (2005). [doi:10.1038/nature04233](https://doi.org/10.1038/nature04233) Medline
4. A. K. Geim, K. S. Novoselov, The rise of graphene. *Nat. Mater.* **6**, 183 (2007). [doi:10.1038/nmat1849](https://doi.org/10.1038/nmat1849) Medline
5. Y. Zhang, Y.-W. Tan, H. L. Stormer, P. Kim, Experimental observation of the quantum Hall effect and Berry's phase in graphene. *Nature* **438**, 201 (2005). [doi:10.1038/nature04235](https://doi.org/10.1038/nature04235) Medline
6. X. Li *et al.*, Graphene-on-silicon Schottky junction solar cells. *Adv. Mater.* **22**,

- 2743 (2010). [doi:10.1002/adma.200904383](https://doi.org/10.1002/adma.200904383)
7. S. Tongay, T. Schumann, A. F. Hebard, Graphite based Schottky diodes formed on Si, GaAs, and 4H-SiC substrates. *Appl. Phys. Lett.* **95**, 222103 (2009). [doi:10.1063/1.3268788](https://doi.org/10.1063/1.3268788)
8. T. Seyller, K. V. Emtsev, F. Speck, K.-Y. Gao, L. Ley, Schottky barrier between 6H-SiC and graphite: Implications for metal/SiC contact formation. *Appl. Phys. Lett.* **88**, 242103 (2006). [doi:10.1063/1.2213928](https://doi.org/10.1063/1.2213928)
9. C.-C. Chen, M. Aykol, C.-C. Chang, A. F. J. Levi, S. B. Cronin, Graphene-silicon Schottky diodes. *Nano Lett.* **11**, 1863 (2011). [doi:10.1021/nl104364c](https://doi.org/10.1021/nl104364c) Medline
10. S. Tongay, T. Schumann, X. Miao, B. R. Appleton, A. F. Hebard, Tuning Schottky diodes at the many-layer-graphene/semiconductor interface by doping. *Carbon* **49**, 2033 (2011). [doi:10.1016/j.carbon.2011.01.029](https://doi.org/10.1016/j.carbon.2011.01.029)
11. L. Bell, W. J. Kaiser, M. H. Hecht, F. J. Grunthaler, Direct control and characterization of a Schottky barrier by scanning tunneling microscopy. *Appl. Phys. Lett.* **52**, 278 (1988). [doi:10.1063/1.99493](https://doi.org/10.1063/1.99493)
12. Y. Xu *et al.*, Inducing electronic changes in graphene through silicon (100) substrate modification. *Nano Lett.* **11**, 2735 (2011). [doi:10.1021/nl201022t](https://doi.org/10.1021/nl201022t) Medline
13. F. Xia, V. Perebeinos, Y. M. Lin, Y. Wu, P. Avouris, The origins and limits of metal-graphene junction resistance. *Nat. Nanotechnol.* **6**, 179 (2011). [doi:10.1038/nnano.2011.6](https://doi.org/10.1038/nnano.2011.6) Medline
14. Y. J. Yu *et al.*, Tuning the graphene work function by electric field effect. *Nano Lett.* **9**, 3430 (2009). [doi:10.1021/nl901572a](https://doi.org/10.1021/nl901572a) Medline
15. A. Reina *et al.*, Large area, few-layer graphene films on arbitrary substrates by chemical vapor deposition. *Nano Lett.* **9**, 30 (2009). [doi:10.1021/nl801827v](https://doi.org/10.1021/nl801827v)
16. K. S. Kim *et al.*, Large-scale pattern growth of graphene films for stretchable transparent electrodes. *Nature* **457**, 706 (2009). [doi:10.1038/nature07719](https://doi.org/10.1038/nature07719) Medline
17. X. Li *et al.*, Large-area synthesis of high-quality and uniform graphene films on copper foils. *Science* **324**, 1312 (2009). [doi:10.1126/science.1171245](https://doi.org/10.1126/science.1171245)

[Medline](#)

18. S. Bae *et al.*, Roll-to-roll production of 30-inch graphene films for transparent electrodes. *Nat. Nanotechnol.* **5**, 574 (2010). [doi:10.1038/nnano.2010.132](#) [Medline](#)
19. I. Jeon *et al.*, Passivation of metal surface states: Microscopic origin for uniform monolayer graphene by low temperature chemical vapor deposition. *ACS Nano* **5**, 1915 (2011). [doi:10.1021/nn102916c](#) [Medline](#)
20. Materials and methods are available as supplementary materials on *Science* Online.
21. C.-H. Liu, C.-C. Wu, Z. Zhong, A fully tunable single-walled carbon nanotube diode. *Nano Lett.* **11**, 1782 (2011). [doi:10.1021/nl200371z](#) [Medline](#)
22. J. Lee, P. P. Gipp, C. M. Heller, Carbon nanotube p-n junction diodes. *Appl. Phys. Lett.* **85**, 145 (2004). [doi:10.1063/1.1769595](#)
23. J. Heo *et al.*, Nonmonotonic temperature dependent transport in graphene grown by chemical vapor deposition. *Phys. Rev. B* **84**, 035421 (2011). [doi:10.1103/PhysRevB.84.035421](#)
24. H. Yabuta *et al.*, High-mobility thin-film transistor with amorphous InGaZnO₄ channel fabricated by room temperature rf-magnetron sputtering. *Appl. Phys. Lett.* **89**, 112123 (2006). [doi:10.1063/1.2353811](#)
25. F. J. Himpsel, G. Hollinger, R. A. Pollak, Determination of the Fermi-level pinning position at Si(111) surfaces. *Phys. Rev. B* **28**, 7014 (1983). [doi:10.1103/PhysRevB.28.7014](#)
26. M. C. Lonergan, A tunable diode based on an inorganic semiconductor–conjugated polymer interface. *Science* **278**, 2103 (1997). [doi:10.1126/science.278.5346.2103](#) [Medline](#)
27. S. W. Boettcher *et al.*, Tunable electronic interfaces between bulk semiconductors and ligand-stabilized nanoparticle assemblies. *Nat. Mater.* **6**, 592 (2007). [doi:10.1038/nmat1943](#) [Medline](#)
28. L. Liao *et al.*, High-speed graphene transistors with a self-aligned nanowire gate. *Nature* **467**, 305 (2010). [doi:10.1038/nature09405](#) [Medline](#)
29. Y.-M. Lin *et al.*, Enhanced performance in epitaxial graphene FETs with optimized channel morphology. *IEEE Electron Device Lett.* **32**, 1343 (2011). [doi:10.1109/LED.2011.2162934](#)

Acknowledgments: The authors are grateful to SAIT colleagues X. Li for TEM analysis assistance and Nano Fabrication group for process assistance. We are also grateful to S.-H. Lee and S. Seo for useful discussions.

Supplementary Materials

www.sciencemag.org/cgi/content/full/science.1220527/DC1

Materials and Methods

Supplementary Text

Figs. S1 to S10

References

14 February 2012; accepted 4 April 2012

Published online 17 May 2012

10.1126/science.1220527